# Instabilities driven equilibration at the early stage of nuclear collisions

Stanislaw Mrówczyński[a]

[a]Institute of Physics, Świętokrzyska Academy,
ul. Świętokrzyska 15, PL - 25-406 Kielce, Poland
and Sołtan Institute for Nuclear Studies,
ul. Hoża 69, PL - 00-681 Warsaw, Poland

Due to anisotropic momentum distribution the parton system produced at the early stage of relativistic heavy-ion collisions is unstable with respect to the magnetic plasma modes. The instabilities isotropize the system and thus speed up the process of its equilibration. The scenario of instabilities driven isotropization is reviewed.

## 1. Introduction

A matter created in relativistic heavy-ion collisions manifests a strongly collective hydrodynamic behaviour [1] which is particularly evident in studies of the so-called elliptic flow [2]. Hydrodynamic description requires, strictly speaking, a local thermal equilibrium and experimental data on the particle spectra and elliptic flow suggest, when analysed within the hydrodynamic model, that an equilibration time of the parton[1] system is as short as 0.6 fm/$c$ [1]. Such a fast equilibration can be explained assuming that the quark-gluon plasma is strongly coupled [3]. However, a high-energy density at the collision early stage, when the elliptic flow is generated, rather suggests that the plasma is then weakly coupled due to the asymptotic freedom. Thus, the question arises whether the weakly interacting plasma can be equilibrated within 1 fm/$c$.

Calculations, which assume that the parton-parton collisions are responsible for the equilibration of the weakly interacting plasma, provide an equilibration time of at least 2.6 fm/$c$ [4]. To thermalize the system one needs either a few hard collisions of the momentum transfer of order of the characteristic parton momentum[2], which is denoted here as $T$ (as the temperature of equilibrium system), or many collisions of smaller transfer. As discussed in *e.g.* [5], the inverse time scale of the collisional equilibration is of order $g^4\ln(1/g)\,T$ where $g$ is the QCD coupling constant. However, the equilibration is speeded up by instabilities generated in an anisotropic quark-gluon plasma [6–8], as growth of the unstable modes is associated with the system's isotropization. The characteristic inverse time of instability development is roughly of order $gT$ for a sufficiently anisotropic

---

[1]The term 'parton' is used to denote quark or gluon.
[2]Although an anisotropic system is considered, the characteristic momentum in all directions is assumed to be of the same order.

momentum distribution [6,9–11]. Thus, the instabilities are much 'faster' than the collisions in the weak coupling regime. Very recent numerical simulation [12] shows that the instabilities driven isotropization is indeed very efficient.

The isotropization should be clearly distinguished from the equilibration. The instabilities driven isotropization is a mean-field reversible phenomenon which is *not* accompanied with the entropy production [6,12]. Therefore, the collisions, which are responsible for the dissipation, are needed to reach the equilibrium state of maximal entropy. The instabilities contribute to the equilibration indirectly, shaping the parton momenta distribution.

A large variety of instabilities of the electron-ion plasma which are known [13]. Those caused by coordinate space inhomogeneities, in particular by the system's boundaries, are usually called *hydrodynamic* instabilities while those due to non-equilibrium momentum distribution of plasma particles are called *kinetic* instabilities. Hardly anything is known about hydrodynamic instabilities of the quark-gluon plasma, and I will not speculate about them. The kinetic instabilities are initiated either by the charge or current fluctuations. In the first case, the electric field ($\mathbf{E}$) is longitudinal ($\mathbf{E} \parallel \mathbf{k}$, where $\mathbf{k}$ is the wave vector), while in the second case the field is transverse ($\mathbf{E} \perp \mathbf{k}$). For this reason, the kinetic instabilities caused by the charge fluctuations are usually called *longitudinal* while those caused by the current fluctuations are called *transverse*. Since the electric field plays a crucial role in the longitudinal mode generation, the longitudinal instabilities are also called *electric* while the transverse ones are called *magnetic*. The magnetic mode known as the filamentaion or Weibel instability appears to be relevant for the quark-gluon plasma produced in relativistic heavy-ion collisions. In the following sections a whole scenario of the instabilities driven isotropization is reviewed.

## 2. Seeds of the filamentation and its mechanism

Let me consider a non-equilibrium parton system which is homogeneous but the parton momentum distribution is anisotropic. The system is on average locally colourless but colour fluctuations are possible. Therefore, $\langle j_a^\mu(x) \rangle = 0$ where $j_a^\mu(x)$ is a local colour four-current in the adjoint representation of SU(3) gauge group with $\mu = 0, 1, 2, 3$ and $a = 1, 2, 3, \ldots, 8$ being the Lorentz and colour index, respectively; $x = (t, \mathbf{x})$ denotes a four-position in the coordinate space. As discussed in [14], the current correlator for a classical system of non-interacting quarks and gluons is

$$M_{ab}^{\mu\nu}(t, \mathbf{x}) \stackrel{\text{def}}{=} \langle j_a^\mu(t_1, \mathbf{x}_1) j_b^\nu(t_2, \mathbf{x}_2) \rangle = \frac{1}{8} g^2 \delta^{ab} \int \frac{d^3 p}{(2\pi)^3} \frac{p^\mu p^\nu}{E_p^2} f(\mathbf{p}) \delta^{(3)}(\mathbf{x} - \mathbf{v}t) , \qquad (1)$$

where $(t, \mathbf{x}) \equiv (t_2 - t_1, \mathbf{x}_2 - \mathbf{x}_1)$ and the effective parton distribution function $f(\mathbf{p})$ equals $n(\mathbf{p}) + \bar{n}(\mathbf{p}) + 6n_g(\mathbf{p})$ with $n(\mathbf{p})$, $\bar{n}(\mathbf{p})$ and $n_g(\mathbf{p})$ giving the average colourless distribution function of quarks $Q^{ij}(x, \mathbf{p}) = \delta^{ij} n(\mathbf{p})$, of antiquarks $\bar{Q}^{ij}(x, \mathbf{p}) = \delta^{ij} \bar{n}(\mathbf{p})$, and of gluons $G^{ab}(x, \mathbf{p}) = \delta^{ab} n_g(\mathbf{p})$. We note that the distribution function of (anti-)quarks belongs to the fundamental representation of the SU(3) gauge while that of gluons to the adjoint representation. Therefore, $i, j = 1, 2, 3$ and $a, b = 1, 2, ..., 8$.

Due to the average space-time homogeneity, the correlation tensor (1) depends only on the difference $(t_2 - t_1, \mathbf{x}_2 - \mathbf{x}_1)$. The space-time points $(t_1, \mathbf{x}_1)$ and $(t_2, \mathbf{x}_2)$ are correlated in the system of non-interacting particles if a particle travels from $(t_1, \mathbf{x}_1)$ to $(t_2, \mathbf{x}_2)$. For
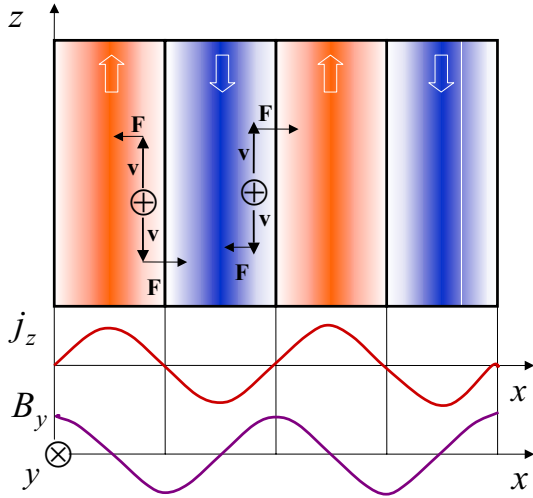
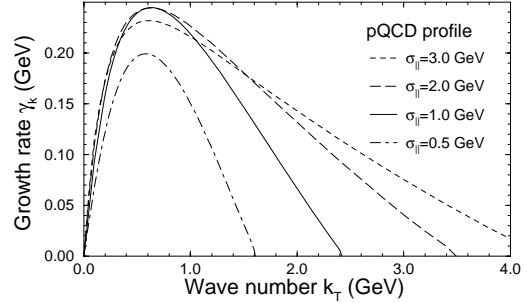Figure 1. The mechanism of filamentation instability, see text for the description.



Figure 2. The growth rate of the unstable mode as a function of the wave vector k $= (k_\perp, 0, 0)$ for $\sigma_\perp = 0.3$ GeV and 4 values of the parameter $\sigma_\parallel$ which controls system's anisotropy. The figure is taken from [9].

this reason the delta $\delta^{(3)}(\mathbf{x} - \mathbf{v}t)$ is present in the formula (1). The momentum integral of the distribution function simply represents the summation over particles. The fluctuation spectrum is found as a Fourier transform of the tensor (1) *i.e.*

$$M_{ab}^{\mu\nu}(\omega, \mathbf{k}) = \frac{1}{8} \, g^2 \, \delta^{ab} \int \frac{d^3 p}{(2\pi)^3} \, \frac{p^\mu p^\nu}{E_p^2} \, f(\mathbf{p}) \, 2\pi\delta(\omega - \mathbf{k}\mathbf{v}) \, . \tag{2}$$

To compute the fluctuation spectrum, the parton momentum distribution has to be specified. Such calculations with two forms of the anisotropic momentum distribution are presented in [14]. Here I only qualitatively discuss Eqs. (1,2). I assume that the momentum distribution is elongated in, say, the $z$ direction. Then, Eqs. (1,2) clearly show that the correlator $M^{zz}$ is larger than $M^{xx}$ or $M^{yy}$. It is also clear that $M^{zz}$ is the largest when the wave vector $\mathbf{k}$ is along the direction of the momentum deficit. Then, the delta function $\delta(\omega - \mathbf{k}\mathbf{v})$ does not much constrain the integral in Eq. (2). Since the momentum distribution is elongated in the $z$ direction, the current fluctuations are the largest when the wave vector $\mathbf{k}$ is the $x-y$ plane. Thus, I conclude that some fluctuations in the anisotropic system are large, much larger than in the isotropic one. An anisotropic system has a natural tendency to split into the current filaments parallel to the direction of the momentum surplus. These currents are seeds of the filamentation instability.

Let me now explain in terms of elementary physics why the fluctuating currents, which flow in the direction of the momentum surplus, can grow in time. To simplify the discussion, which follows [14], I consider an electromagnetic anisotropic system. The form of the fluctuating current is chosen to be

$$\mathbf{j}(x) = j \, \hat{\mathbf{e}}_z \cos(k_x x) \, , \tag{3}$$

where $\hat{\mathbf{e}}_z$ is the unit vector in the $z$ direction. As seen in Eq. (3), there are current filaments of the thickness $\pi/|k_x|$ with the current flowing in the opposite directions in the

neighbouring filaments. The magnetic field generated by the current (3) and the Lorentz force acting on the partons, which fly along the $z$ direction, are given as

$$\mathbf{B}(x) = \frac{j}{k_x}\,\hat{\mathbf{e}}_y \sin(k_x x)\;, \qquad \mathbf{F}(x) = q\,\mathbf{v}\times\mathbf{B}(x) = -q\,v_z\,\frac{j}{k_x}\,\hat{\mathbf{e}}_x \sin(k_x x)\;,$$

where $q$ is the electric charge. One observes, see Fig. 1, that the force distributes the partons in such a way that those, which positively contribute to the current in a given filament, are focused in the filament centre while those, which negatively contribute, are moved to the neighbouring one. Thus, the initial current grows. For a somewhat different explanation see [11].

## 3. Dispersion equation

The equation of motion of the Fourier transformed chromodynamic field $A^\mu(k)$ is

$$\left[k^2 g^{\mu\nu} - k^\mu k^\nu - \Pi^{\mu\nu}(k)\right]A_\nu(k) = 0\;, \tag{4}$$

where $\Pi^{\mu\nu}(k)$ is the polarization tensor or gluon self-energy which is discussed later on. A general plasmon dispersion equation is of the form

$$\det\left[k^2 g^{\mu\nu} - k^\mu k^\nu - \Pi^{\mu\nu}(k)\right] = 0\;. \tag{5}$$

Due to the transversality of $\Pi^{\mu\nu}(k)$ ($k_\mu\Pi^{\mu\nu}(k) = k_\nu\Pi^{\mu\nu}(k) = 0$) not all components of $\Pi^{\mu\nu}(k)$ are independent from each other, and consequently the dispersion equation (5), which involves a determinant of $4 \times 4$ matrix, can be simplified to the determinant of $3 \times 3$ matrix. For this purpose, I introduce the chromoelectric permittivity tensor $\epsilon^{lm}(k)$ where the indices $l, m, n = 1, 2, 3$ label three-vector and tensor components. Because $\epsilon^{lm}(k)E^l(k)E^m(k) = \Pi^{\mu\nu}(k)A_\mu(k)A_\nu(k)$, where $\mathbf{E}$ is the chromoelectric vector, the permittivity can be expressed through the polarization tensor as $\epsilon^{lm}(k) = \delta^{lm} + \Pi^{lm}(k)/\omega^2$. Then, the dispersion equation gets the form

$$\det\left[\mathbf{k}^2\delta^{lm} - k^l k^m - \omega^2\epsilon^{lm}(k)\right] = 0 \tag{6}$$

and the permittivity tensor $\epsilon^{lm}(k)$, which can be derived either within the transport theory or diagrammatically [15], is

$$\epsilon^{nm}(\omega,\mathbf{k}) = \delta^{nm} + \frac{g^2}{2\omega}\int\frac{d^3p}{(2\pi)^3}\frac{v^n}{\omega - \mathbf{k}\mathbf{v} + i0^+}\frac{\partial f(\mathbf{p})}{\partial p^l}\left[\left(1 - \frac{\mathbf{k}\mathbf{v}}{\omega}\right)\delta^{lm} + \frac{k^l v^m}{\omega}\right]\;. \tag{7}$$

Since $\Pi^{\mu\nu}(k)$ and $\epsilon^{lm}(k)$ are unit matrices in the colour space, the colour indices are suppressed here.

Substituting the permittivity (7) into Eq. (6), one fully specifies the dispersion equation (6) which provides a spectrum of quasi-particle bosonic excitations. A solution $\omega(\mathbf{k})$ of Eq. (6) is called *stable* when $\mathrm{Im}\,\omega \leq 0$ and it is called *unstable* when $\mathrm{Im}\,\omega > 0$. In the first case the amplitude is constant or it exponentially decreases in time while in the second one there is an exponential growth of the amplitude. In practice, it appears difficult to find solutions of Eq. (6) because of rather complicated structure of the tensor (7). A quite general analysis of the dispersion equation of anisotropic system is given in [10].
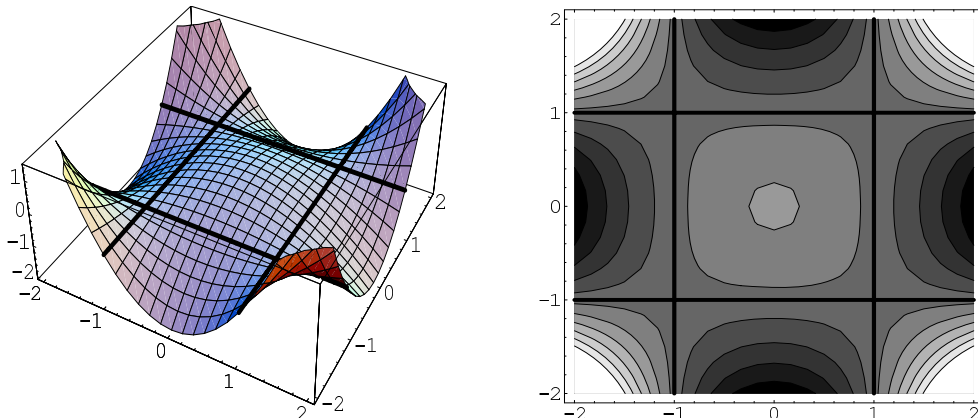
Figure 3. The effective potential of the unstable magnetic mode as a function of magnitude of two colour components of $\mathbf{A}^a$ belonging to the SU(2) gauge group. The figure is taken from [17].

The problem simplifies as we are interested in specific modes which are expected to be unstable. Namely, we look for solutions corresponding to the fluctuating current in the direction of the momentum surplus and the wave vector perpendicular to it.

As previously, the momentum distribution is assumed to be elongated in the $z$ direction, and consequently the fluctuating current also flows in this direction. The magnetic field has a non-vanishing component along the $y$ direction and the electric filed in the $z$ direction. Finally, the wave vector is parallel to the axis $x$, see Fig. 1. It is also assumed that the momentum distribution obeys the mirror symmetry $f(-\mathbf{p}) = f(\mathbf{p})$, and then the permittivity tensor has only non-vanishing diagonal components. Taking into account all these conditions, one simplifies the dispersion equation (6) to the form

$$H(\omega) \equiv k_x^2 - \omega^2 \epsilon^{zz}(\omega, k_x) = 0 . \tag{8}$$

An existence of unstable solutions of Eq. (8) can be proved without solving it. The so-called Penrose criterion [13], which follows from analytic properties of the permittivity as a function of $\omega$, states that *the dispersion equation $H(\omega) = 0$ has unstable solutions if $H(\omega = 0) < 0$*. The Penrose criterion was applied to the equation (8) in [6] but a much more general discussion of the instability condition is presented in [11]. Not entering into details, there exist unstable modes if the momentum distribution averaged (with a proper weight) over momentum length is anisotropic.

To solve the dispersion equation (8), the parton momentum distribution has to be specified. Several analytic (usually approximate) solution of the dispersion equation can be found in [6,10,11]. A typical example of the numerical solution, which gives the unstable mode frequency in the full range of wave vectors is shown in Fig. 2 taken from [9]. The mode is pure imaginary and $\gamma_k \equiv \mathrm{Im}\,\omega(k_\perp)$. The parameters $\sigma_\parallel$ and $\sigma_\perp$ control the widths of longitudinal ($z$) and transverse momentum distributions; the coupling is $\alpha_s \equiv g^2/4\pi = 0.3$, and the effective parton density is chosen to be 6 fm$^{-3}$. As seen, there is a finite interval of wave vectors for which the unstable modes exist.
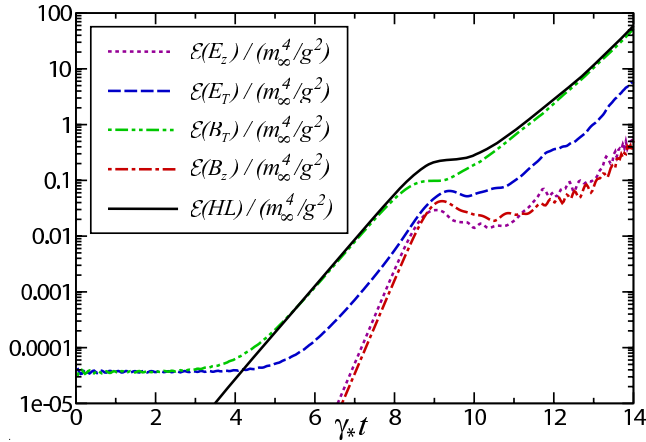
Figure 4. Time evolution of the (scaled) energy density (split into various electric and magnetic components) which is carried by the chromodynamic field. The simulation is 1+1 dimensional and the gauge group is SU(2). The parton momentum distribution is squeezed along the $z$ axis. The solid line corresponds to the total energy transferred from the particles. The figure is taken from [7].
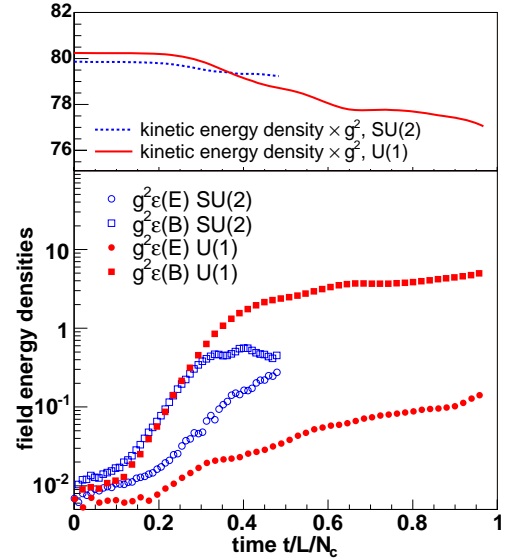
Figure 5. Time evolution of the kinetic energy of particles (upper panel) and of the energy of electric and magnetic fields (lower panel) in GeV/fm$^3$ for the U(1) and SU(2) gauge groups. The figure is taken from [12].

## 4. Isotropization and Abelianization

When the instabilities grow the system becomes more isotropic because the Lorentz force changes particle's momenta and the growing fields curry an extra momentum. To explain the mechanism I assume, as previously, that initially there is a momentum surplus in the $z$ direction. The fluctuating current tends to flow in the $z$ direction with the wave vector pointing in the $x$ direction. Since the magnetic field has a $y$ component, the Lorentz force, which acts on partons flying along the $z$ axis, pushes the partons in the $x$ direction where there is a momentum deficit. Numerical simulations discussed in the next section show the efficiency of the mechanism.

The system isotropizes not only due to the effect of the Lorentz force but also due to the momentum carried by the growing field. When the magnetic and electric fields are oriented along the $y$ and $z$ axes, respectively, the Poynting vector points in the direction $x$ that is along the wave vector. Thus, the momentum carried by the fields is oriented in the direction of the momentum deficit of particles.

Unstable modes cannot grow to infinity and even in the electron-ion plasma there are several possible mechanisms which stop the growth [16]. In the case of the quark-gluon plasma one suspects that non-Abelian non-linearities can play an important role here. An elegant argument [17] suggests that the non-linearities do not stabilize the unstable modes because the system spontaneously chooses an Abelian configuration in the course of instability development. Let me explain the idea.
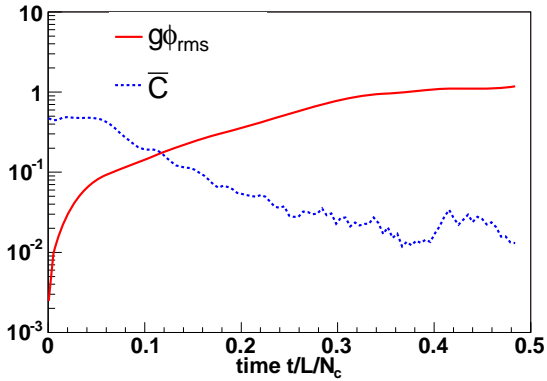
Figure 6. Temporal evolution of the functionals $\bar{C}$ and $\phi_{\mathrm{rms}}$ measured in GeV. The figure is taken from [12].
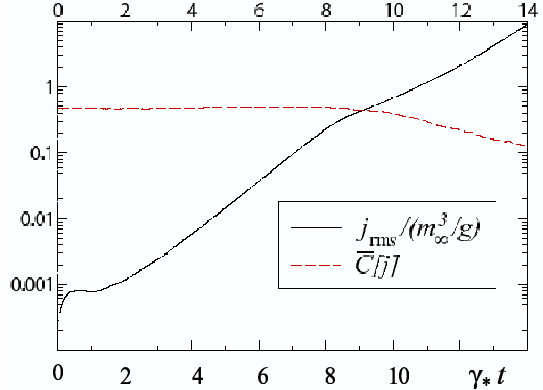


Figure 7. Temporal evolution of the (scaled) functionals $\bar{C}$ and $j_{\mathrm{rms}}$. The figure is taken from [7].

In the Coulomb gauge the effective potential of the unstable configuration has the form

$$V_{\mathrm{eff}}[\mathbf{A}^a] = -\mu^2 \mathbf{A}^a \cdot \mathbf{A}^a + \frac{1}{4}g^2 f^{abc} f^{ade}(\mathbf{A}^b \mathbf{A}^d)(\mathbf{A}^c \mathbf{A}^e) \, ,$$

which is shown in Fig. 3 taken from [17]. The first term (with $\mu^2 > 0$) is responsible for a very existence of the instability. The second term, which comes from the Yang-Mills lagrangian, is of pure non-Abelian nature. The term is positive and thus it counteracts the instability growth. However, the non-Abelian term vanishes when the potential $\mathbf{A}^a$ is effectively Abelian, and consequently, such a configuration corresponds to the steepest decrease of the effective potential. Thus, the system spontaneously abelianizes in the course of instability growth. The abelianization is further discussed in the next section.

## 5. Numerical simulations

Temporal evolution of the anisotropic quark-gluon plasma has been recently studied by means of numerical simulations [7,12,18,19]. The dynamics governed by a complete Hard Loop action, which for anisotropic systems was derived in [20], has been simulated in [7,18,19]. These simulations provide fully reliable information on the field dynamics but particles are included as a stationary (anisotropic) background. The simulation [12] treats the quark-gluon system completely classically: partons, which curry classical colour charges, interact with a self-consistently generated classical chromodynamic field. The simulations [7,12] have been effectively performed in 1+1 dimensions as the chromodynamic potentials depend on time and one space variable. The calculations [18,19] represent full 1+3 dimensional dynamics. In most cases the SU(2) gauge group was studied but some SU(3) results, which are qualitatively very similar to SU(2) ones, are given in [19]. The techniques of discretization used in [7,12,18,19] are rather different while the initial conditions are quite similar. The initial field amplitudes are distributed according to the Gaussian noise and the momentum distribution of partons is strongly anisotropic.

In Fig. 4, taken from [7], the results of the Hard-Loop simulation performed in 1+1 dimensions are shown. One observes exponential growth of the field energy density which
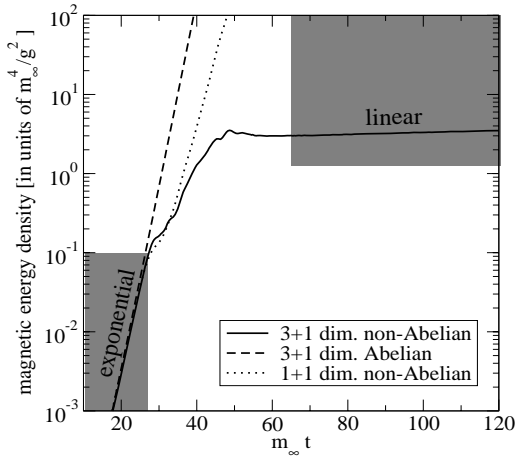
Figure 8. Time evolution of the (scaled) chromomagnetic energy density in the 1+3 dimensional simulation. The Abelian result and that of 1+1 dimensions are also shown. The figure is taken from [18].
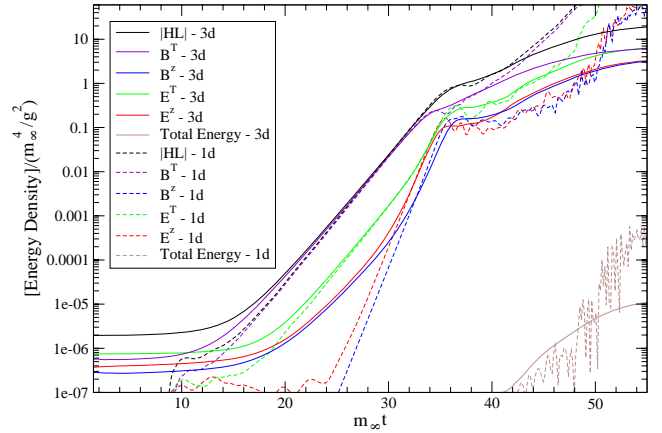


Figure 9. Time evolution of the (scaled) energy density (split into various electric and magnetic components) of the chromodynamic field in the 1+1 and 1+3 simulations. 'HL' denotes the total energy contributed by hard particles. The figure is taken from [19].

is dominated, as expected, by the magnetic field which is transverse to the direction of the momentum deficit. The growth rate appears to be equal to that of the fastest unstable mode ($\gamma^*$). Fig. 5, taken from [12], shows results of the classical simulation on the 1+1 dimensional lattice of physical size $L = 40$ fm. As in Fig. 4, the amount of field energy grows exponentially and the magnetic contribution dominates.

The Abelian (U(1)) and nonAbelian (SU(2)) results of the 1+1 dimensional simulation presented in Fig. 5 are remarkably similar to each other. The abelianization appears to be very efficient in 1+1 dimensions, as shown in Figs. 6, 7, taken from [12] and [7], respectively. The authors of [12] analysed the functionals:

$$\phi_{\rm rms} \equiv \sqrt{\int_0^L \frac{dx}{L}(A_y^a A_y^a + A_z^a A_z^a)} \,, \qquad \bar{C} \equiv \int_0^L \frac{dx}{L} \frac{\sqrt{{\rm Tr}[(i[A_y, A_z])^2]}}{{\rm Tr}[A_y^2 + A_z^2]} \,. \qquad (9)$$

The quantities $j_{\rm rms}$ and $\bar{C}$, studied in [7] and shown in Fig. 7, are fully analogous to $\phi_{\rm rms}$ and $\bar{C}$ defined by Eq. (9) but the components of chromodynamic potential are replaced by the respective components of the colour current. As seen in Figs. 6, 7, the field (current) commutator decreases in time although the magnitude of field (current), as quantified by $\phi_{\rm rms}$ ($j_{\rm rms}$), grows.

The results of the 1+3 dimensional simulations [18,19] are qualitatively different from those of 1+1 dimensions. As seen in Figs. 8, 9, taken from [18,19], respectively, the growth of the field energy density is exponential only for some time, and then the growth becomes approximately linear. The regime changes when the field's amplitude is of order $k/g$ where $k$ is the characteristic wave vector. Then, the nonAbelian effects start to be important. Fig. 10 taken from [18] demonstrates that the abelianization is efficient in 1+3 dimensions only for a finite interval of time. The commutator $C$ shown in Fig. 10 is a natural generalization of the 1+1 dimensional commutator defined by Eq. (9).
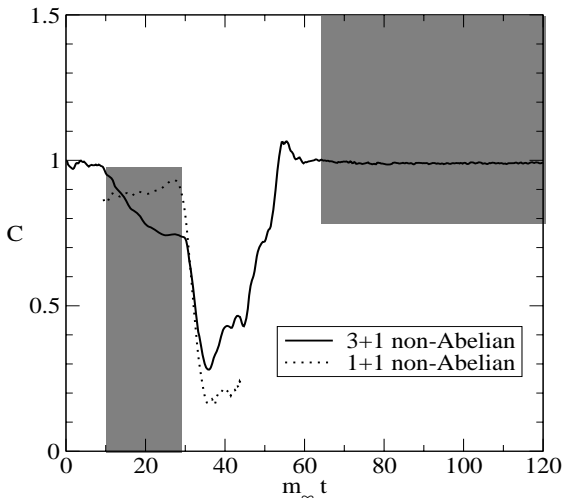
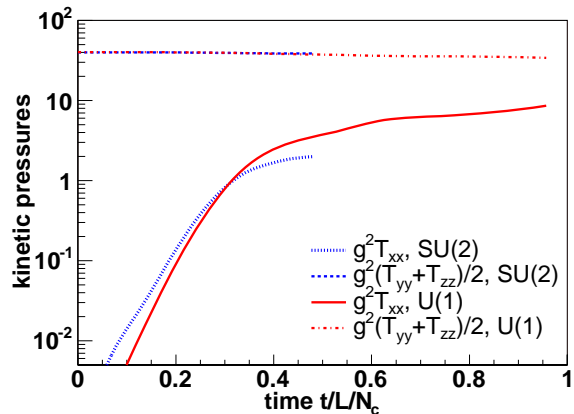Figure 10. Temporal evolution of the field commutator quantified by $C$. The figure is taken from [18].



Figure 11. Temporal evolution of the energy-momentum tensor components $T^{xx}$ and $(T^{yy} + T^{zz})/2$. The Abelian and non-Abelian results are shown. The figure is taken from [12].

The effect of isotropization due to the action of the Lorentz force is nicely seen in the 1+1 dimensional classical simulation [12]. In Fig. 11 taken from [12] there are shown diagonal components of the energy-momentum tensor $T^{\mu\nu}$. The initial momentum distribution is such that $T^{xx} = 0$ at $t = 0$. As seen, $T^{xx}$ exponentially grows.

## 6. Outlook

One wonders whether the instabilities are experimentally observable in nuclear collisions. The accelerated equilibration is only an indirect signal. Strong chromomagnetic fields generated by the instabilities have been suggested [21,22] to provide a specific pattern of jet's deflections. This promising signal obviously needs further studies.

Another idea has been proposed in [23]. The quark-gluon plasma, which is locally isotropic, manifests, as argued in [8], an approximate hydrodynamic behaviour. The azimuthal fluctuations can presumably distinguish the approximate hydrodynamics from the real hydrodynamics describing a system in local equilibrium. Non-equilibrium fluctuations are usually significantly larger than the equilibrium fluctuations of the same quantity. Thus, the fluctuations of $v_2$ produced in the course of real hydrodynamic evolution are expected to be significantly smaller than those generated in the non-equilibrium isotropic plasma. A much simple integral measurement of azimuthal fluctuations can also help to distinguish the equilibrium from non-equilibrium fluctuations [23].

Although an impressive progress has been achieved, the numerical simulations [7,12, 18,19] are still quite far from a real situation met in relativistic heavy-ion collisions. The effect of back reaction of fields on the particles is fully included only in the classical 1+1 dimensional simulation [12]. The 1+3 dimensional simulations are needed as the results of [18,19] show that the dimensionality crucially matters. The system's expansion, which can cut off instability growth [9], also needs to be included.

Understanding of a late stage of the instability growth, when fields are of large mag-

nitude, is a real theoretical challenge. A mechanism of instability saturation is not well known even in the electron-ion plasma [16]. Non-linear effects, in particular those of non-Abelian nature, are then essential. Except the classical simulation [12], the evolution of anisotropic quark-gluon plasma has been studied within the Hard Loop approximation. An attempt to go beyond it has been undertaken in [24] where the higher order terms of the effective potential of the anisotropic system have been found. Since these terms can be negative, the instability is then driven not only by the negative quadratic term but by the higher order terms as well. However, before a real progress in the strong field domain can be achieved, one needs a better insight into the Hard Loop dynamics which has appeared to be very reach [18,19].

In summary, the magnetic instabilities provide a plausible explanation of a surprisingly short equilibration time observed in relativistic heavy-ion collisions. Fast isotropization is a distinctive feature of the mechanism.

**REFERENCES**

1.  U. W. Heinz, AIP Conf. Proc. **739** (2005) 163.
2.  F. Retiere, J. Phys. G **30** (2004) S827.
3.  E. Shuryak, J. Phys. G **30** (2004) S1221.
4.  R. Baier, A. H. Mueller, D. Schiff and D. T. Son, Phys. Lett. B **539** (2002) 46.
5.  P. Arnold, D. T. Son and L. G. Yaffe, Phys. Rev. D **59** (1999) 105020.
6.  St. Mrówczyński, Phys. Rev. C **49** (1994) 2191.
7.  A. Rebhan, P. Romatschke and M. Strickland, Phys. Rev. Lett. **94** (2005) 102303.
8.  P. Arnold, J. Lenaghan, G. D. Moore and L. G. Yaffe, Phys. Rev. Lett. **94** (2005) 072302.
9.  J. Randrup and St. Mrówczyński, Phys. Rev. C **68** (2003) 034909.
10. P. Romatschke and M. Strickland, Phys. Rev. D **68** (2003) 036004.
11. P. Arnold, J. Lenaghan and G. D. Moore, JHEP **0308** (2003) 002.
12. A. Dumitru and Y. Nara, Phys. Lett. B **621** (2005) 89.
13. N.A. Krall and A.W. Trivelpiece, *Principles of Plasma Physics* (McGraw-Hill, New York, 1973).
14. St. Mrówczyński, Phys. Lett. B **393** (1997) 26.
15. St. Mrówczyński and M. H. Thoma, Phys. Rev. D **62** (2000) 036011.
16. T. N. Kato, Phys. Plasmas **12** (2005) 080705.
17. P. Arnold and J. Lenaghan, Phys. Rev. D **70** (2004) 114007.
18. P. Arnold, G. D. Moore and L. G. Yaffe, arXiv:hep-ph/0505212.
19. A. Rebhan, P. Romatschke and M. Strickland, arXiv:hep-ph/0505261.
20. St. Mrówczyński, A. Rebhan and M. Strickland, Phys. Rev. D **70** (2004) 025004.
21. M. Strickland, private comunication.
22. B. Müller, arXiv:nucl-th/0508062.
23. St. Mrówczyński, arXiv:hep-ph/0506179.
24. C. Manuel and St. Mrówczyński, Phys. Rev. D **72** (2005) 034005.